Surface & Coatings Technology 253 (2014) 241–248

Contents lists available at ScienceDirect

Surface & Coatings Technology

journal homepage: www.elsevier.com/locate/surfcoat

Bronze electrodeposition from an acidic non-cyanide high efficiency electrolyte: Tribological behavior

L.N. Bengoa [a,b], W.R. Tuckart [c], N. Zabala [c], G. Prieto [c], W.A. Egli [a,*]

[a] Center for Paints and Coatings Development–CICBA-CONICET, Av. 52 e/121 y 122, La Plata, Argentina
[b] School of Engineering, Universidad Nacional de La Plata, Av.1 y 47, La Plata, Argentina
[c] Tribology Group, Engineering Department, Universidad Nacional del Sur–CONICET, Av. Alem 1253, 1° Piso, 8000 Bahía Blanca, Bs. As., Argentina

ARTICLE INFO

Article history:
Received 6 November 2013
Accepted in revised form 25 May 2014
Available online 2 June 2014

Keywords:
Bronze
Electrodeposition
Cyanide-free electrolyte
Tribology
Wear resistance

ABSTRACT

Bronze coatings were electrodeposited onto a rotating cylinder electrode from a novel non-cyanide acid plating bath with high efficiency (92%). Deposits were obtained from a phenol sulfonic acid bath and their morphology, phase composition and tribological behavior were characterized. Cyclic and linear sweep voltammetries were used to study the effect of organic additives on the reduction processes to achieve an adequate formulation. The resulting bronze deposit consisted of a mono α-phase matrix with a 78% Cu and 22% Sn composition. Dry sliding wear tests were carried out employing a homemade ball on ring system and the coefficient of friction and wear resistance were quantified at different normal loads. Surface characterization of the bronze coatings showed that the resulting roughness is detrimental for the wear resistance of the deposit. This is evidenced by a higher friction coefficient and wear volume of Cu/Sn compared to a conventionally electrodeposited copper coating.

© 2014 Elsevier B.V. All rights reserved.

1. Introduction

Electrodeposited Cu–Sn alloys, commonly known as bronze, are widely used as protective and decorative coatings due to their good corrosion resistance and appearance [1,2]. For several years bronze plating has been carried out in an alkaline cyanide-based electrolyte [1–4], which produces high quality deposits but causes several environmental problems, during use and disposal, owing to its high toxicity [5]. The latter, together with increasing environmental regulations, have encouraged the development of a large number of cyanide-free baths for Cu–Sn alloys electrodeposition.

Most formulations reported so far have been achieved by the addition of a tin salt to electrolytes used for copper plating. Among these, sulfate solutions containing organic additives have been by far the most widely studied [6–13], though some pyrophosphate-based [14] and non-cyanide alkaline baths have also been developed [15]. In all these cases the addition of such organic compounds is necessary to attain high quality bronze coatings. For example, surface active substances, mainly polyethers or polyesters, are added as they act as wetting agents and inhibitors (leveling agents) [7,8] producing smooth surfaces. In addition, a second organic substance containing double bonds or aromatic rings is usually used as a brightener to obtain lustrous coatings [8,16]. Such is the case of benzyl alcohol (BA), which has been used to obtain bright bronze coatings with 20% of tin [13], and benzaldehyde, whose effect on sulfate electrolytes has been studied by Survila et al. [8]. Regardless the vast variety of organic compounds that have been evaluated, there are some common features that can be remarked. One of them is the deposition of tin at potentials less cathodic than the equilibrium reduction potential of Sn^{+2}, which can be attributed to an under potential deposition (UPD) mechanism. The other one is related to the formation of various bronze phases, stable only at high temperatures, whose content in the deposit strongly depends on the electrodeposition conditions [17].

Although good quality bronze coatings have been plated from sulfate solutions, these electrolytes have a major drawback: an important loss of tin by spontaneous oxidation of Sn^{+2} as SnO_2 [9,13,18]. An alternative to overcome this problem is the development of new baths based on commercially used tin plating electrolytes, which have been formulated taking this issue into consideration. Some authors have already considered the use of methane sulfonic acid (MSA) as a suitable electrolyte for Cu–Sn alloys deposition [19,20]. Another chemistry which has been used for decades in tinplate production, is the phenol sulfonic acid (PSA) based electrolyte [21–23]. It is worth noting that the electrolyte's formulation usually includes a surface active substance as an additive. One of them is Diphone VI (D6), a sulfonate compound containing aromatic rings. It is important to recall that little attention has been paid to additives with such a structure and their effect on Cu–Sn electrodeposition process.

As has been mentioned, bronze deposits have several uses as protective and decorative coatings. In addition, they have been proposed as an alternative to copper coatings in some industrial applications due to

* Corresponding author. Tel.: +54 221 483 1141; fax: +54 221 427 1537.
E-mail address: anelpire3@cidepint.gov.ar (W.A. Egli).

http://dx.doi.org/10.1016/j.surfcoat.2014.05.046
0257-8972/© 2014 Elsevier B.V. All rights reserved.

their higher hardness. For example, Cu–Sn alloys electrodeposited from a cyanide electrolyte have proved to be a suitable option when plating threaded joints [24], which means that these coatings are able to withstand high loads for short times without undergoing galling. Although many authors have studied the electrodeposition of Cu–Sn from non-cyanide electrolytes, little efforts have been put in evaluating the mechanical performance of the resulting deposits.

The present paper deals with the study of Cu–Sn alloys electrodeposition from a PSA based electrolyte to which small amounts of BA are added. Special attention was paid to the mechanical and tribological properties of the resulting coatings in order to evaluate their performance at similar experimental conditions as those found during the make-up and break-out of threaded joints.

2. Materials and methods

PSA electrolytes were prepared for electrodeposition of Cu/Sn alloys. PSA and Sn^{+2} concentrations were similar to those usually found in tin-plating industry [22,23,25], while Cu^{+2} concentration was defined considering values found in the literature for the deposition of bronze from acid baths [6–13]. The chemicals used to prepare the baths and their concentrations are listed in Table 1.

Cyclic voltammetry (CV) and linear sweep voltammetry (LSV) were carried out using an EG&G Princeton Applied Research Potentiostat/Galvanostat (Mod. 273A) coupled to a personal computer controlled by CorrWare2® software. The working electrode was a Pt rotating disk electrode (RDE), with an active surface area of 0.041 cm^2, while the counter electrode was a Pt wire (1.6 cm^2). A standard saturated calomel electrode (SCE) was used as reference electrode and all the electrochemical potential values in this work are expressed in this scale. The potential window examined was between −0.75 V and 0.15 V vs SCE. All CV curves were recorded at a scan rate of 20 mV/s and 500 rpm. In contrast, LSV was performed at several scan rates (1–20 mV/s) and rotation speeds (100–1500 rpm) to identify the charge-transfer and mass-transport controlled processes. The temperature was fixed at (30 ± 0.2 °C). Galvanostatic deposits were obtained on low carbon steel rotating cylinder electrodes (RCE) 5 cm long and 0.8 cm diameter. This geometry was chosen to meet the requirements of the homemade ball on ring system used in the tribological experiments (described later). Before plating, the steel substrates were electrochemically degreased in a 30 g/L NaOH solution at a cathodic current density of 64 A/dm^2 at room temperature and then pickled in 10% sulfuric acid at 70 ºC. A very thin deposit of nickel (nickel strike) was electrodeposited on the steel cylinders before co-deposition of tin and copper to avoid the Cu^{+2} cementation reaction. To that end, a Woods solution (240 g/L $NiCl_2 \cdot 6H_2O$, 126 mL/L HCl) was prepared and electrodeposition was carried out at room temperature for 3 min at 13 A/dm^2 [26]. For tin–copper electrodeposition a copper anode was used instead of a bronze one because of the short electrolysis time of each experiment and the relative high tin concentration in the electrolyte. During galvanostatic deposition experiments, the cathode was rotated at 500 or 800 rpm and the temperature was set to a value of (30 ± 0.2 °C). Current density was varied between 2.5 and 3.75 A/dm^2 and the electrodeposition time was adjusted to obtain approximately 50 μm thick deposits. For reference, some cylinders were coated with copper using a traditional sulfate bath containing 117.9 g/L $CuSO_4 \cdot 5H_2O$, 120 g/L H_2SO_4 and 70 ppm Cl^-. These samples were plated at the same temperature and rotation speed used in the other experiments, while the current density was set at 8 A/dm^2.

SEM micrographs were recorded with a Quanta200 FEI equipment (Tungsten filament source). The composition of the coatings was evaluated using EDS. XRD spectra of the coatings were determined with an equipment Phillips X'Pert diffractometer with a CuKα = 1.5405 Å. The detector scan mode with a step size of 0.05° and a sampling time of 3 s was used (scan rate 0.0167 º/s). Coating surface roughness was evaluated according to ISO 3274:1996 by means of a profilometer Hommel Etamic T500 and Etamic software. In addition, hardness measurements were made with a Vickers microhardness measuring device. The reported values for each sample are the results of at least 10 measurements.

Samples were embedded in an epoxy resin and mechanically ground with 800 to 2500 grade silicon paper. Finally, the samples were polished with 6 μm and 1 μm diamond paste and faradaic efficiency (FE) of the electrolytes was quantified through coating thickness measurements from optical micrographs of the cross sections.

Dry sliding wear tests were carried out by employing a homemade ball on ring system. The coated samples were rotated at a constant speed of 12 rpm (0.3 m/s) against a 6.35 mm diameter SAE 52100 steel ball used as the counter-body. The contact load was 5 and 10 N of normal force and the total sliding distance was of 170 cm. These experimental conditions were carefully chosen with the aim of reproducing the industrial make up and break out process. All the sliding wear experiments were run in a controlled environment: (25 ± 1 °C) and 50%–55% relative humidity. Wear quantification was achieved measuring the width of wear track from optical microscopy (OM) images and the coating volume damage was calculated assuming that the counter-body remains unchanged. The reported results are an average of at least two tests. COF was recorded during the test and the value was defined according to standard ASTM G 115-04.

3. Results and discussion

3.1. Cu/Sn alloy electrodeposition

LSVs of Cu^{+2}, Sn^{+2} and mixed Cu^{+2}/Sn^{+2} in a PSA electrolyte are shown in Fig. 1. For the Cu^{+2} solution, copper deposition starts at approximately $E_{Cu} = 0.12$ V. Once Cu^{+2} discharge begins, the current density increases reaching a limiting current plateau at an electrode potential of $E = -0.26$ V. On the other hand, for the Sn^{+2} electrolyte, tin reduction does not occur until the electrode potential reaches a value of $E_{Sn} = -0.47$ V. A similar value for tin discharge in an MSA electrolyte was reported by Pewnim and Roy [19]. At approximately $E = -0.50$ V a small shoulder can be appreciated, after which the current rises linearly. A similar behavior was observed by Wen and Szpunar [27] who attributed the peak to the existence of a nucleation and growth mechanism controlled by mass transfer.

When both ions are present in the solution the reduction process starts at $E_{CuSn} = -0.04$ V, which is more cathodic than the deposition

Table 1
Chemicals used and their concentrations in the bath.

Chemical component	Nomenclature	Concentration in the bath
$SnSO_4$ Sigma-Aldrich 95%	–	0.253 mol dm^{-3}
$CuSO_4 \cdot 5H_2O$ Cicarelli 100%	–	0.063–0.126–0.189 mol dm^{-3}
Phenol sulfonic acid (acidity 234.53 gr H_2SO_4/L)	PSA	0.115 mol dm^{-3}
Diphone VI	D6	8 g/L
Benzyl alcohol Fisher Scientific 99%	BA	3 mL/L

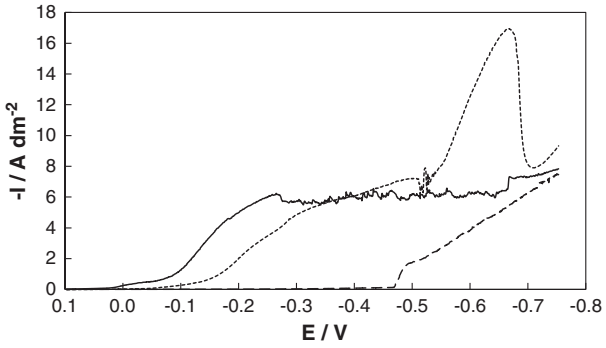

Fig. 1. LSV of (- - -) 0.253 mol dm^{-3} $SnSO_4$, (—) 0.126 mol dm^{-3} $CuSO_4$ and (····) 0.253 mol dm^{-3} $SnSO_4$ + 0.126 mol dm^{-3} $CuSO_4$ in 0.115 mol dm^{-3} PSA containing D6, recorded at 5 mV/s and 500 rpm.

potential of Cu^{+2} (E_{Cu}). This suggests that the addition of stannous tin inhibits to some extent the reduction of copper. In Fig. 1, it is clearly seen that the current density of the Cu–Sn system is smaller than the current of the Cu^{+2} reduction up to $E = -0.40$ V. In the potential region $-0.46 < E < -0.40$ the current density associated to the copper process has already reached its limiting value. Thus, the higher current value observed for the Cu–Sn solution can be the result of UPD of tin as has been already stated [6–8,17]. Another peculiarity of the Cu–Sn voltammogram is the appearance of current oscillations at $E \approx -0.50$ V. Such phenomenon has been observed before during copper and tin electrodeposition from a sulfate electrolyte and has been related to the existence of two different thermodynamically stable states between which the system oscillates [9]. The adsorption of surface active substances onto the electrode resulting in process inhibition has been proposed as one possible cause of this behavior. Finally, when the potential becomes more cathodic a further rise in current density occurs, probably due to tin electrodeposition, and a peak is formed at $E_p = -0.64$ V (peak I), after which the current drops sharply. A further increase in current density may be attributed to hydrogen evolution which, according to various authors, starts at $-0.60 \text{ V} < E < -0.70$ V in Cu–Sn electrolytes [7,10,20].

Fig. 2 shows the effect of BA on the reduction of the individual components as well as on the cathodic processes of Cu–Sn co-deposition. It can be seen that this additive does not affect significantly the partial deposition processes of copper and tin. However, a slight increase in tin reduction current was registered, which was also verified by an increase in tin dissolution peak height during CV (not shown). In the presence of both components BA only modifies the electrochemical response at $E < -0.50$ V, making oscillations more intense (bigger amplitude) and strongly inhibiting peak I. It is also worth noting that, even though oscillations were present in the absence of BA, the abrupt drop in current density a $E = -0.50$ V was only observed when this additive was added. All these results are indicative of a simultaneous interaction among BA, Sn^{+2} and Cu^{+2}, and discard the existence of strong BA–Sn^{+2} and BA–Cu^{+2} interactions.

To understand better the role of BA in the deposition of Cu–Sn alloys, solutions without D6 were prepared and LSV curves were recorded. The results obtained (Fig. 3) show that BA reduces somewhat the current density at $E < -0.64$ V, slightly inhibiting tin deposition. Comparison of Figs. 1, 2 and 3 leads to the conclusion that the effect of BA on the cathodic phenomena is stronger in the presence of D6. Such a synergetic effect between additives was also observed before by Survila et al. [8]. Furthermore, it shows that peak I is generated only when D6 is added to the bath and that this additive also polarizes the initiation of the cathodic process.

The effect of copper concentration was studied by LSV and CV. LSV curves shown in Fig. 4 indicates that the current plateau in the region $-0.50 \text{ V} < E < -0.30$ V corresponds to a mass transfer controlled process related to Cu reduction. This kind of behavior was observed both in the presence (Fig. 4-a) and in the absence (Fig. 4-b) of BA. Furthermore, an increase in $CuSO_4$ concentration from 0.063 to 0.189 mol dm^{-3} shifts the peak I position in 130 mV in the cathodic direction (Fig. 4-a). This suggests that copper intervenes in the deposition process taking place at the peak, which may be under diffusion control. Another interesting feature is that Cu^{+2} concentration has almost no effect on the current values registered at $E < -0.63$ V when BA is added to the solution. Thus, it is likely that in the presence of BA, processes occurring in this potential region are not under mass transfer control.

CV curves (Fig. 5) show that raising the copper concentration reduces the Sn dissolution peak and, in contrast, increases the Cu dissolution peak height. The latter divides into two peaks ($E \approx 0.20$ V and $E \approx 0.37$ V) when $CuSO_4$ concentration reaches a value of 0.189 mol dm^{-3}, which could be attributed to the formation of a second Cu-rich phase or even free Cu based on the position of copper dissolution peak measured by CV (not shown). The charge per unit area for each peak was estimated using data fitting tools and the quotient Q_{Sn}/Q_{Cu} was calculated. The values obtained are 1.6, 0.6 and 0.3 for $CuSO_4$ concentrations of 0.063, 0.126 and 0.189 mol dm^{-3}, respectively. These results show that the co-deposition of copper and tin is more balanced when the copper salt concentration is 0.126 mol dm^{-3}. Thus, further experiments in this work were carried out under this condition.

In order to confirm the diffusional nature of the several processes observed, LSVs were recorded at different rotation speeds and sweep rates, keeping the copper concentration at a fixed value. As was expected, for $E > -0.50$ V the effect of rotation speed on the LSV shape is equivalent to that of Cu^{+2}concentration both in the absence and presence of BA. The current density of the plateau increases with rotation rate of

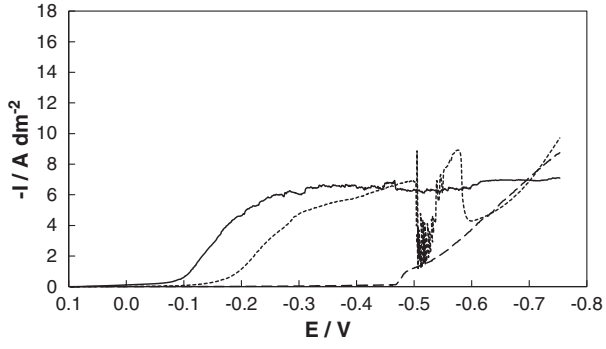

Fig. 2. LSV of (- - -) 0.253 mol dm^{-3} $SnSO_4$, (—) 0.126 mol dm^{-3} $CuSO_4$ and (····) 0.253 mol dm^{-3} $SnSO_4$ + 0.126 mol dm^{-3} $CuSO_4$ in 0.115 mol dm^{-3} PSA containing D6 and BA, recorded at 5 mV/s and 500 rpm.

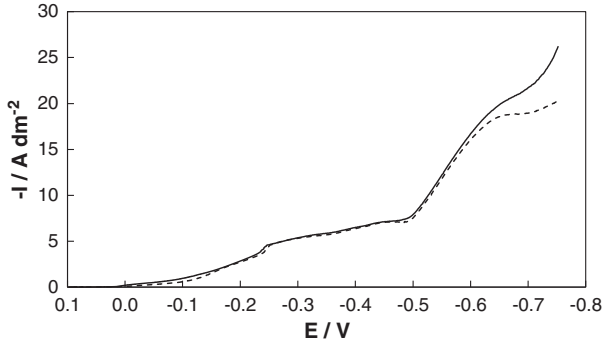

Fig. 3. LSV of 0.253 mol dm^{-3} $SnSO_4$ + 0.126 mol dm^{-3} $CuSO_4$ in 0.115 mol dm^{-3} PSA without D6, with (- - -) and without (—) BA, recorded at 5 mV/s and 500 rpm.

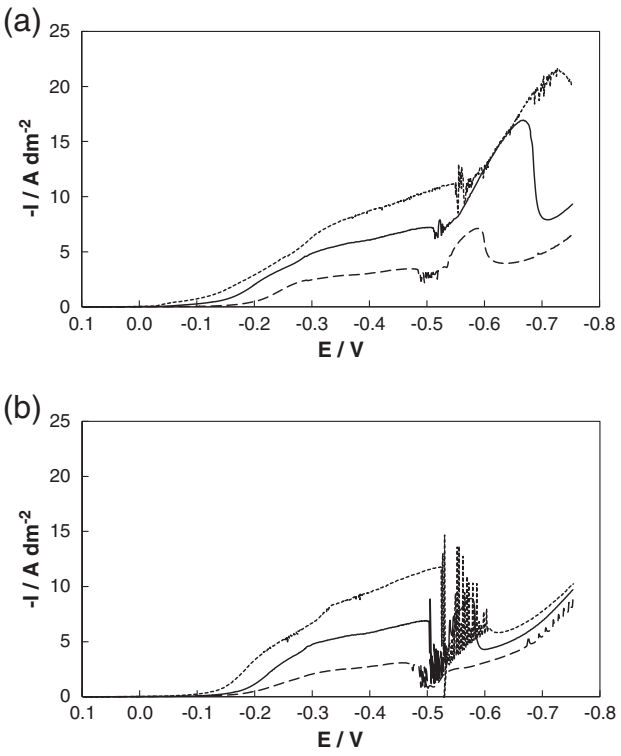

Fig. 4. LSV of (- - -) 0.063 mol dm^{-3} $CuSO_4$, (—) 0.126 mol dm^{-3} $CuSO_4$ and (····) 0.253 mol dm^{-3} $CuSO_4$ in 0.115 mol dm^{-3} PSA containing D6 and 0.253 mol dm^{-3} $SnSO_4$, (a) without BA and (b) with BA. A scan rate of 5 mV/s was used and the rotation speed was 500 rpm.

the electrode in accordance with Levich equation (Fig. 6). It is worth noting that the slope of this plateau is more pronounced than that expected for an electrochemical reaction under diffusion control. The reason of this phenomenon is the onset of Sn^{+2} deposition at potentials less cathodic than its reduction potential (UPD) [6]. It was also found that with the addition of BA to the bath, the LSV curve for $E < -0.50$ V does not vary with the angular speed of the electrode (not shown), confirming the non-diffusional nature inferred from Fig. 4-b.

LSV recorded at different sweep rates shows that increasing the sweep rate from 1 mV/s to 20 mV/s exerts no influence in a solution

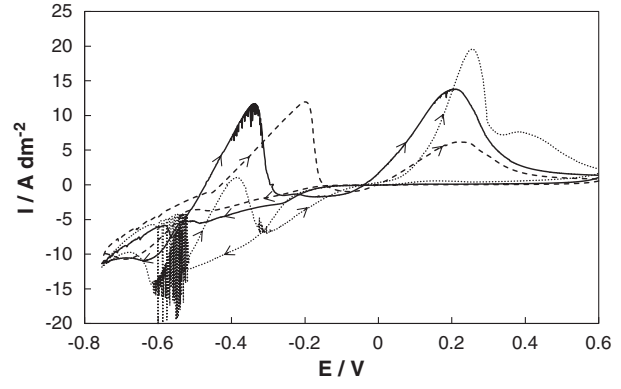

Fig. 5. CV of (- - -) 0.063 mol dm^{-3} $CuSO_4$, (—) 0.126 mol dm^{-3} $CuSO_4$ and (····) 0.253 mol dm^{-3} $CuSO_4$ in 0.115 mol dm^{-3} PSA containing D6 and 0.253 mol dm^{-3} $SnSO_4$, with the addition of BA. A scan rate of 20 mV/s was used and the rotation speed was 500 rpm.

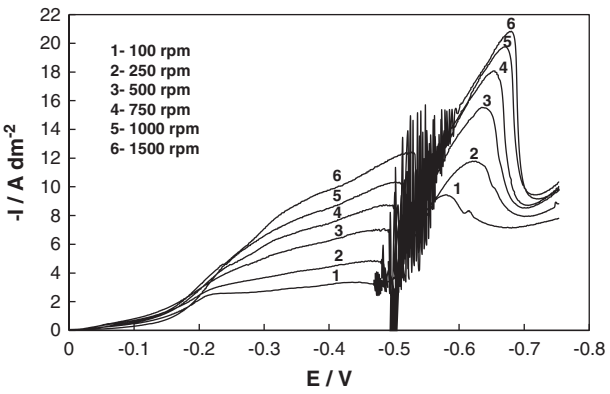

Fig. 6. CV of 0.253 mol dm^{-3} $SnSO_4$ + 0.126 mol dm^{-3} $CuSO_4$ in 0.115 mol dm^{-3} PSA containing D6, obtained at several rotation speeds between 100 and 1500 rpm. RDE speed is indicated at curve. The scan rate was set at 20 mV/s.

without BA (Fig. 7). The latter can be concluded as the current density and the peak I position remains virtually unchanged. When the additive is added a strong inhibition of peak I is observed, whose position and current now depend on sweep rate (Fig. 8). It is seen that the peak height decreases as the sweep rate increases until it disappears at 20 mV/s. Based on these results, it can be assumed that the peak corresponds to a slow process in which Cu^{+2} and Sn^{+2} take part when both D6 and BA are present in the electrolyte. Another important feature of these curves is that oscillations at $E = -0.50$ V become more intense at high sweep rate, as opposed to the behavior reported by other authors [9].

To clarify the effect of BA on the process occurring at E_p, potentiostatic deposits were obtained at this value. The Sn content in the deposit increased from 23 wt% to 35 wt% as a result of the addition of this additive. This is in agreement with the increase in tin deposition observed when BA is added to a solution containing Sn^{+2} only, which was mentioned previously. It also suggests that this organic compound can be used to produce coatings with high tin contents. However, to fully understand the mechanism through which Cu–Sn co-deposition occurs further studies are needed.

To evaluate the properties of the coatings plated from a bath containing BA, galvanostatic deposits onto a RCE were obtained out at various experimental conditions. These, together with the coatings composition, are summarized in Table 2. A highly dendritic coating

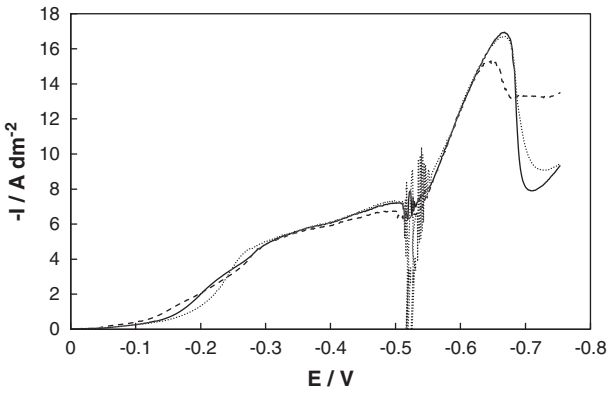

Fig. 7. LSV of 0.253 mol dm^{-3} $SnSO_4$ + 0.126 mol dm^{-3} $CuSO_4$ in 0.115 mol dm^{-3} PSA containing D6, recorded at (- - -) 1 mV/s, (—) 5 mV/s and (····) 20 mV/s. Rotation speed: 500 rpm.

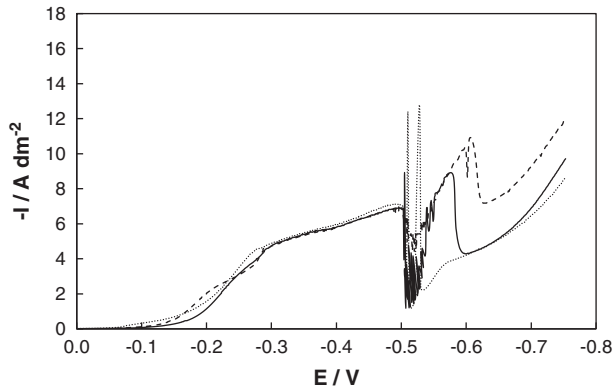

Fig. 8. LSV of 0.253 mol dm^{-3} $SnSO_4$ + 0.126 mol dm^{-3} $CuSO_4$ in 0.115 mol dm^{-3} PSA containing D6 and BA, recorded at (- - -) 1 mV/s, (—) 5 mV/s and (····) 20 mV/s. Rotation speed: 500 rpm.

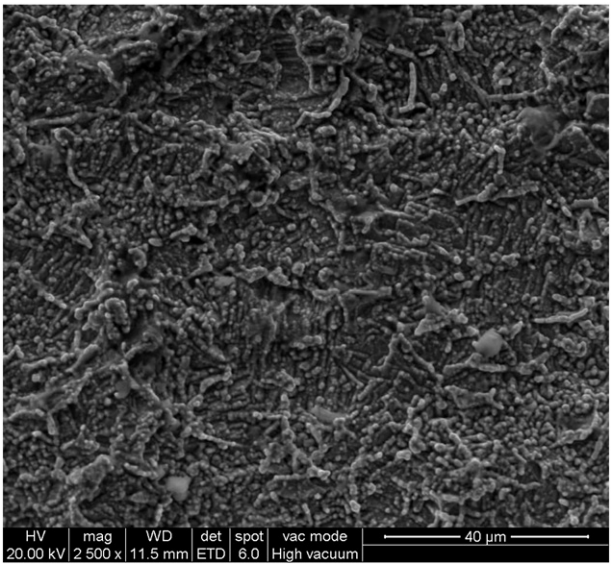

Fig. 9. SEM image of bronze coating (Deposit III). 2500×.

was obtained when the copper concentration in the electrolyte was low (Deposit I). Dendritic growth occurs when the current density is close to the limiting current density and diffusion control governs the electrode reaction. Under these conditions, the deposition rate is higher at the protuberances of a coarse surface because there, the thickness of the diffusion layer is smaller. This leads to an increase of the surface roughness and, if a critical overpotential is reached, to the formation of dendrites [28–31]. Thus, to avoid this unwanted effect the limiting current density for copper deposition was increased by raising Cu^{+2} concentration [32]. This also reduces the tin content in the deposit (Deposit II), if the current density is kept constant, as it enlarges the Cu deposition rate (see Fig. 5). To overcome this effect, current density was increased leading to the production of a smooth, homogeneous and yellow (Deposit III). The increase in tin content can be understood considering that Sn^{+2} reduction is not under mass-transfer while Cu^{+2} is (Fig. 4-b). Then, raising the current density results in an increase in Sn deposition rate, while copper reduction remains almost constant. A further deposit was obtained at a higher rotation speed (Deposit IV), resulting in a lower tin content. The latter is probably a consequence of the relationship between the limiting current density of Cu^{+2} and the electrode rotation rate aforementioned.

Due to its good properties and its high amount of tin (22 wt% Sn), Deposit III was consider for further analysis. SEM images (Fig. 9) reveal an irregular surface morphology with little globular peaks. Moreover, the XRD spectra of this coating (Fig. 10) show that it consists of a mono α-phase copper–tin alloy [3,17]. FE for the deposition of this alloy gave an average of 92%. Fig. 11-a shows a cross section of this bronze coating. It can be seen that it has a very irregular topography, with large rounded peaks and plateau-like protuberances, while copper exhibits a smoother surface, and a more uniform thickness (Fig. 11-b). These results indicate that the cyanide-free electrolyte could produce fair quality bronze coatings at high FE, similar to other industrial electrolytic baths. However, further investigations on process variables sensitivity are needed.

Table 2
Experimental conditions and coatings composition for RCE deposits.

Deposit	I (A/dm^2)	$CuSO_4$ (mol dm^{-3})	Rotation speed (rpm)	Cu (wt %)	Sn (wt %)
I	2.50	0.063	500	90.6	9.4
II	2.50	0.126	500	92.2	7.8
III	3.75	0.126	500	78.1	21.9
IV	3.75	0.126	800	91.6	8.4

3.2. Tribological behavior

An overview of the characteristics of the Cu/Sn and Cu coatings is presented in Table 3. The hardness of bronze coatings was 372 HV, which suggests a priori that the electroplated alloy should have an improved wear resistance. It can be seen that the bronze deposit has a higher roughness causing a more irregular contact between the surfaces during sliding. This is responsible for the lower performance of the Cu/Sn coating at 5 N load and accounts for the noisy COF vs. time curves (Fig. 12-a), due to asperity interlocking [33]. This phenomenon also leads to wider wear scars because of vibration and contact discontinuity. Thus, these results were not taken into account for volume loss calculations.

The bronze coated sample showed a COF value between 0.2 and 0.5 at 5 N. When the load was doubled the COF values were lower and more stable during the whole test. It is also evident that the measurements were noisier for the alloy than for the pure Cu deposit (Fig. 12-b). Fig. 13-d shows a significant amount of transferred material from the bronze coating to the counter-body. This phenomenon is responsible for the increase in the friction coefficient toward the end

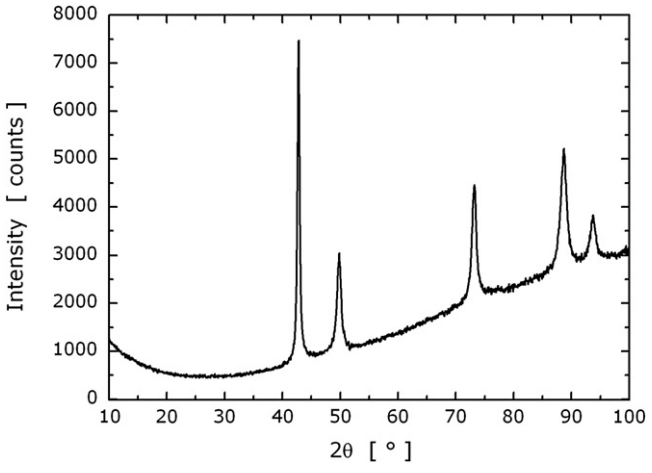

Fig. 10. XRD spectra of bronze coating (Deposit III).

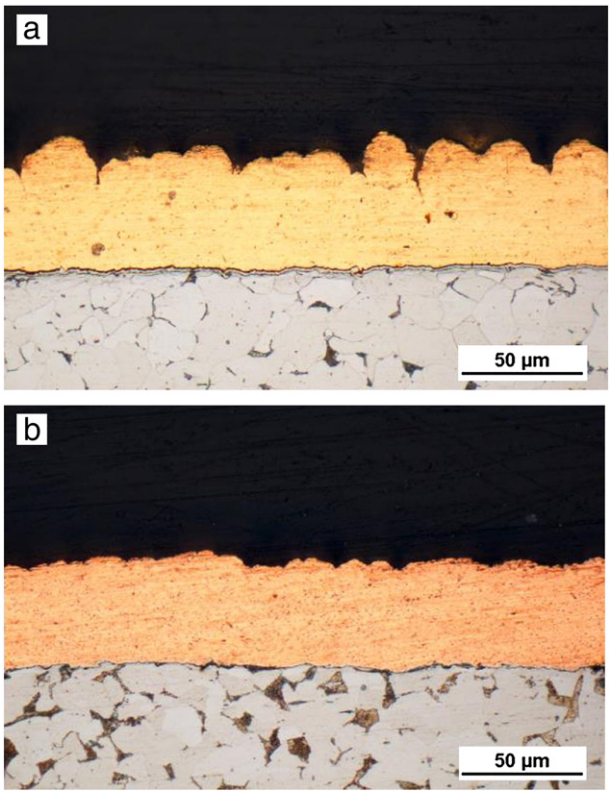

Fig. 11. OM image at 500 of a cross section of (a) Cu/Sn deposit and (b) Cu deposit.

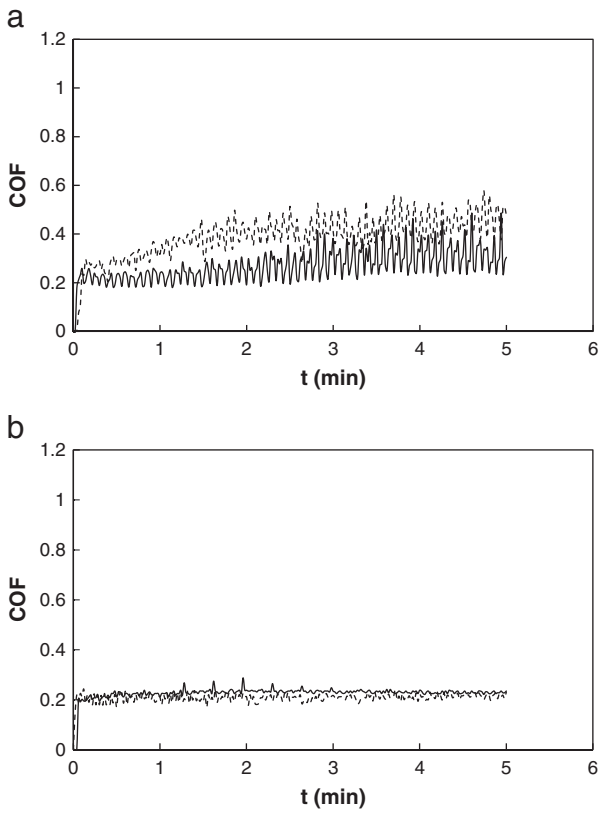

Fig. 12. COF as a function of time at 5 N (- - -) and 10 N (—) loadings. (a) Cu/Sn coating. (b) Cu coating.

of the test, due to the development of large adhesion forces between the surfaces. Guo et al. [34] reported that friction coefficient was increased with increasing Sn content, therefore supporting the different friction behavior exhibited by the two coatings. At 10 N normal load, the high roughness level of the coated surface led to the severe deformation and break-off of the protruding peaks, thus accounting for the higher wear loss compared to copper.

A very different behavior was exhibited by the Cu coating, which showed a low and steady COF value for both load regimes. Due to the ratio between the hardness of the copper coating and of the counter-body, contact pressure is expected to remain below the shakedown limit [35] of the material, therefore leading to mild wear.

Thus, it can be seen that the acting wear mechanism is different for each coating. Due to the selected experimental conditions, the bronze coating has not been able to complete the running-in stage, whereas copper does, reaching a steady-state at a mild wear level.

OM images of the tribosurfaces for the two types of coatings are shown in Figs. 13 and 14. Fig. 14-c shows a wear track in a Cu coated sample under a load of 10 N, in which adhesive wear can be observed. The appearance of brim-like shapes is an indicative of plastic deformation of the superficial layer. It is also interesting to note that some worn asperity peaks can be seen near the main wear track, meaning that a full steady-state was not reached during the test. In this case, the coating is softer than the steel substrate and the counter-body, leading to the developing of ploughing under both load regimes [36], as it can be seen in Fig. 14-a and c. As ploughing develops, contact pressure tends to reduce, leading to a mild wear regime.

For the bronze coatings, at 5 N of applied normal load (Fig. 13-a), only the crests of the protruding peaks of the coating surface are worn, while a smoother and more uniform wear pattern is observed for the higher load (10 N), as it can be seen in Fig. 13-c.

Even though contact pressure at 5 N seems to be insufficient to reach the plastic shakedown limit, it is high enough to promote asperities to fracture and transfer from the coating to the hard counter-body (Fig. 13-b). Under this condition, a steady-state is reached at high COF values due to adhesion between the coating and the transferred layer.

At 10 N asperities undergo severe plastic deformation, therefore lowering the contact pressure below the shakedown limit [37]. This condition is characterized by mild wear rates, as it can be seen in Fig. 13-c and d. Ploughing in this case is dominated by the substrate fracture toughness, which is assumed to be much lower than that of the hard counter-body [38]. A COF reduction for higher load levels and a gradual increase in wear depth with the normal applied load have also been reported by Alam et al. [39] while studying friction and wear characteristics of aluminum bronze coatings.

Track width and wear volume results obtained for each type of coating are shown in Table 4. It can be seen that even though the bronze coating is harder than copper, it has an increased friction coefficient and lower wear resistance, as it can be observed when comparing worn volumes for each coating.

Table 3
Overview of roughness, thickness and Vickers micro hardness.

Coating	Roughness parameter [μm]			Thickness [μm]	Microhardness $HV_{0.01}$
	R_a	R_z	R_t		
Cu/Sn	4.2 ± 0.6	26.1 ± 4.0	46.9 ± 1.4	48.0 ± 3.7	372 ± 5
Cu	1.2 ± 0.1	11 ± 0.1	8.6 ± 0.1	40.0 ± 1.0	160 ± 4

4. Conclusions

Bronze coatings containing up to a 22% wt can be deposited from a PSA-based electrolyte containing $CuSO_4$ and $SnSO_4$ and Diphone VI and benzyl alcohol as additives. Voltammetric data show that, in the

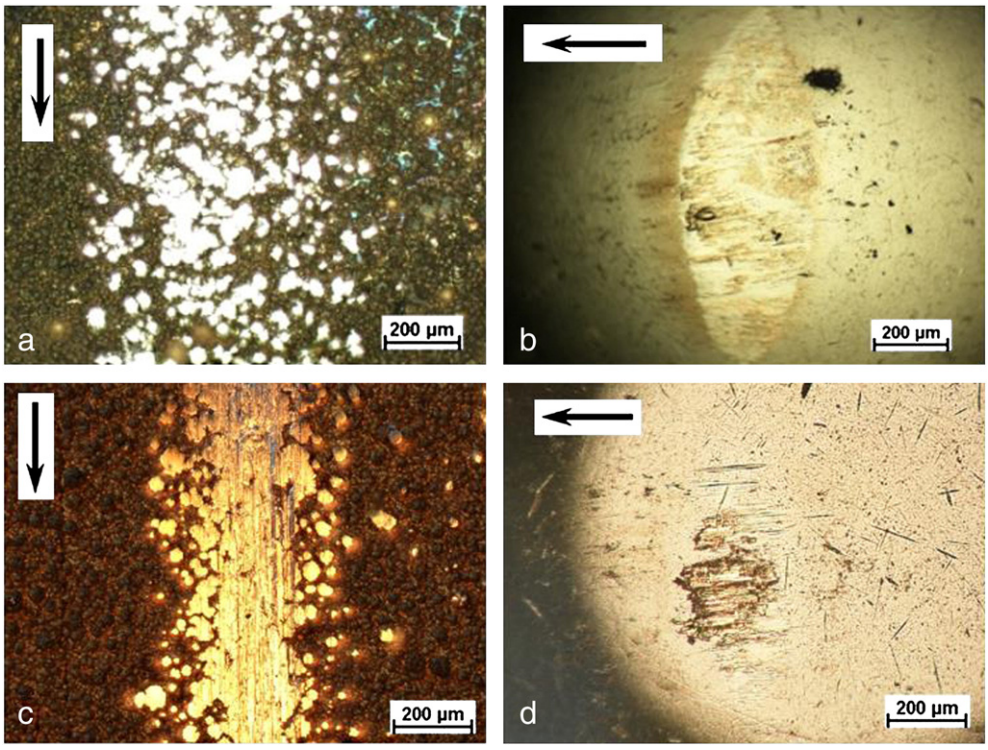

Fig. 13. OM image of Cu/Sn coating and steel ball counter body tested at 5 N (a, b) and 10 N (c, d) loadings.

presence of D6, BA strongly influences the electrochemical process when both metal ions are present. This additive also enhances Sn deposition as was verified by CV and EDS analysis. In contrast, when D6 is not present a slight inhibition of tin reduction was observed. The fact that BA exerts an intense effect on the co-deposition process only in the presence of D6 can be attributed to the existence of a synergism between these two additives. This is also supported by an increase in current oscillations registered at $E = -0.50$ V, which may be the result of an adsorption phenomenon. However, further investigations need to be carried out in order to understand the complex processes taking place in these systems.

Galvanostatic deposition experiments on a RCE show that the coating composition and morphology depend on rotation speed, current density and Cu^{+2}/Sn^{+2} concentration in the solution. Adjusting the electroplating

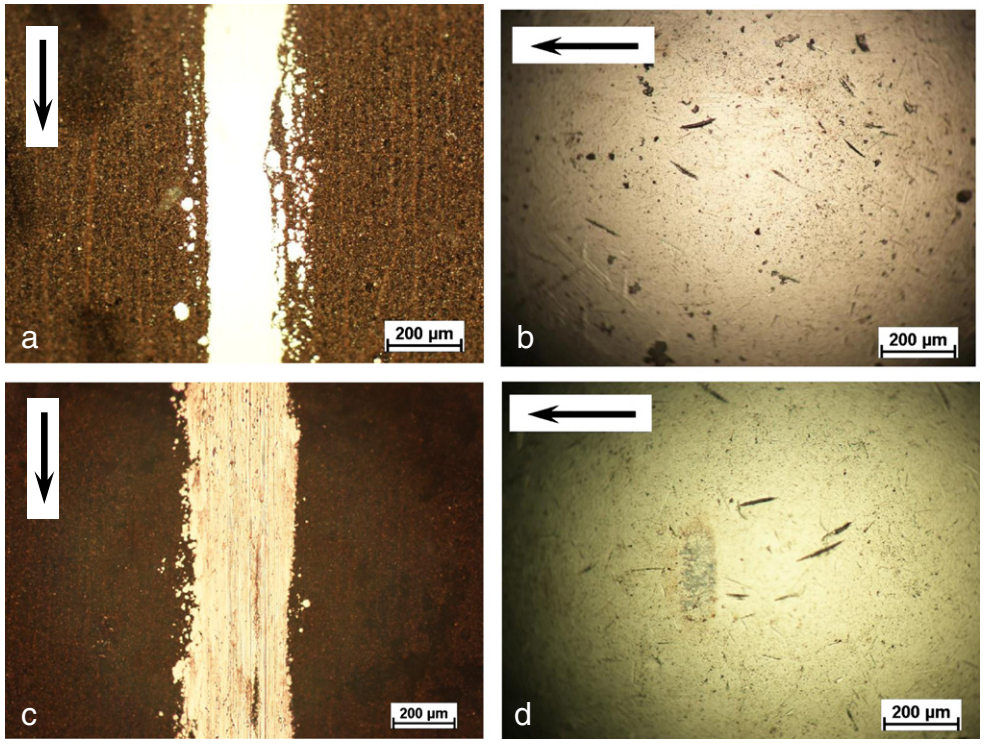

Fig. 14. OM images of Cu coating and steel ball counter body tested at 5 N (a, b) and 10 N (c, d) loadings.

Table 4
COF and wear volumes obtained from the tests made at 5 N and 10 N.

Coating	Applied load			
	5 N		10 N	
	COF	Wear volume [mm^3]	COF	Wear volume [mm^3]
Cu/Sn	0.40	–	0.25	0.93 ± 0.1
Cu	0.20	0.33 ± 0.7	0.22	0.63 ± 0.1

conditions, bronze coatings containing up to a 22%wt can be obtained at high efficiencies (92%). These deposits consist of a mono α-phase Cu/Sn alloy matrix and have a very irregular topography, with large rounded peaks and plateau-like protuberances.

The tribological tests show that even though the bronze coating is harder than copper, it has a greater friction coefficient and lower wear resistance, which is a result of the high surface roughness of the deposits. Thus, although the proposed methodology made possible the electrodeposition of thick bronze deposits using a more environmentally friendly bath, the resulting surface morphology needs to be further improved in order to enhance the tribological behavior of the coating. This subject is going to be addressed in a future study.

Acknowledgments

The authors thank the Comisión de Investigaciones Científicas de la Provincia de Buenos Aires (CICPBA), Consejo Nacional de Investigaciones Científicas y Técnicas (CONICET) and Universidad Nacional de La Plata (UNLP) and Universidad Nacional del Sur (UNS) for their financial support to this research.

References

[1] H. Strow, Met. Finish. 97 (1999) 206–209.
[2] Surf. Eng.ASM International, 1994, p. 257.
[3] A. Afshar, M. Ghorbani, M. Mazaheri, Surf. Coat. Technol. 187 (2004) 293–299.
[4] T. Nickchi, M. Ghorbani, Surf. Coat. Technol. 203 (2009) 3037–3043.
[5] N. Piccinini, G.N. Ruggiero, G. Baldi, A. Robotto, J. Hazard. Mater. 71 (2000) 395–407.
[6] A. Survila, Z. Mockus, S. Kanapeckaite, V. Jasulaitiene, R. Juškenas, J. Electroanal. Chem. 647 (2010) 123–127.
[7] A. Survila, Z. Mockus, S. Kanapeckaite, V. Jasulaitiene, R. Juškenas, Electrochim. Acta 52 (2007) 3067–3074.
[8] A. Survila, Z. Mockus, S. Kanapeckaite, V. Jasulaitiene, R. Juškenas, J. Appl. Electrochem. 39 (2009) 2021–2026.
[9] A. Survila, Z. Mockus, R. Juškenas, Electrochim. Acta 43 (1997) 909–917.
[10] Z. Mockus, O. Galdikienė, J. Appl. Electrochem. 24 (1994) 1009–1012.
[11] I.A. Carlos, C.A.C. Souza, E.M.J.A. Pallone, R.H.P. Francisco, V. Cardoso, B.S. Lima-Neto, J. Appl. Electrochem. 30 (2000) 987–994.
[12] E.P. Barbano, G.M. de Oliveira, M.F. de Carvalho, I.A. Carlos, Surf. Coat. Technol. 240 (2014) 14–22.
[13] G.I. Medvedev, N.A. Makrushin, O.V. Ivanova, Russ. J. Appl. Chem. 77 (2004) 1104–1107.
[14] A.N. Correia, M.X. Façanha, P.d. Lima-Neto, 201 (2007) 7216-7221.
[15] G.A. Finazzi, E.M.d. Oliveira, I.A. Carlos, Surf. Coat. Technol. 187 (2004) 377–387.
[16] G.I. Medvedev, N.A. Makrushin, A.N. Dubenkov, Russ. J. Appl. Chem. 75 (2002) 1799–1803.
[17] R. Juškėnas, Z. Mockus, S. Kanapeckaitė, G. Stalnionis, A. Survila, Electrochim. Acta 52 (2006) 928–935.
[18] D. Thomson, D.A. Luke, C. Mosher, US 5,378,347, 1995.
[19] N. Pewnim, S. Roy, Electrochim. Acta 90 (2013) 498–506.
[20] C.T.J. Low, F.C. Walsh, Surf. Coat. Technol. 202 (2008) 1339–1349.
[21] M. Schlesinger, M. Paunovic, Modern electroplating, 5th ed. John Wiley & Sons, New Jersey, 2010. 153–154.
[22] C.H. O'driscoll, European Patent EP0857226 B1, 2001.
[23] E. Morgan, in: E. Morgan (Ed.), Tinplate & Modern Canmaking Technology, Pergamon, Oxford, 1985, pp. 5–73.
[24] R.J. Guise, M.G. Edwards, US 7,472,927 B2, 2009.
[25] Y.-H. Yau, J. Electrochem. Soc. 147 (2000) 1071–1076.
[26] ASTM International, West Conshohocken, PA, 2009.
[27] S. Wen, J.A. Szpunar, Electrochim. Acta 50 (2005) 2393–2399.
[28] K.I. Popov, M.G. Pavlovic, M.D. Maksimovic, J. Appl. Electrochem. 12 (1982) 525–531.
[29] K.I. Popov, N.V. Krstajić, M.I. Čekerevac, in: R.E. White, B.E. Conway, J.O.M. Bockris (Eds.), Modern aspects of electrochemistry, Plenum Press, New York, 1996, pp. 261–312.
[30] K.I. Popov, S.S. Djokić, B.N. Grgur, Fundamental aspects of electrometallurgy, Kluwer Academic/Plenum Publishers, New York, 2002, pp. 29–100.
[31] K.I. Popov, N.D. Nikolic, in: S.S. Djokić (Ed.), Electrochemical production of metal powders, Springer Science+Business Media, New York, 2012, pp. 1–62.
[32] J.O.M. Bockris, A.K.N. Reddy, Modern electrochemistry, Plenum Press, New York, 1970. 991–1140.
[33] K. Holmberg, H. Ronkainen, A. Matthews, Ceram. Int. 26 (2000) 787–795.
[34] X. Guo, G. Zhang, W. Li, L. Dembiski, Y. Gao, H. Liao, C. Coddet, Appl. Surf. Sci. 254 (2007) 1482–1488.
[35] A. Kapoor, Wear 212 (1997) 119–130.
[36] K. Holmberg, A. Matthews, H. Ronkainen, Tribol. Int. 31 (1998) 107–120.
[37] A. Kapoor, J.A. Williams, K.L. Johnson, Wear 175 (1994) 81–92.
[38] K. Holmberg, H. Ronkainen, A. Laukkanen, K. Wallin, Surf. Coat. Technol. 202 (2007) 1034–1049.
[39] S. Alam, S. Sasaki, H. Shimura, Wear 248 (2001) 75–81.